ACS APPLIED ENERGY MATERIALS

www.acsaem.org Article

High Energy Density Lithium−Sulfur Batteries Based on Carbonaceous Two-Dimensional Additive Cathodes

Julen Castillo, Alexander Santiago,* Xabier Judez, Jose Antonio Coca-Clemente, Amaia Saenz de Buruaga, Juan Luis Gómez-Urbano, Jose Antonio González-Marcos, Michel Armand, Chunmei Li,* and Daniel Carriazo

Cite This: *ACS Appl. Energy Mater.* 2023, 6, 3579−3589 Read Online

ACCESS | Metrics & More | Article Recommendations | Supporting Information

ABSTRACT: The increasing demand for electrical energy storage makes it essential to explore alternative battery chemistries that overcome the energy-density limitations of the current state-of-the-art lithium-ion batteries. In this scenario, lithium−sulfur batteries (LSBs) stand out due to the low cost, high theoretical capacity, and sustainability of sulfur. However, this battery technology presents several intrinsic limitations that need to be addressed in order to definitively achieve its commercialization. Herein, we report the fruitfulness of three different formulations using well-selected functional carbonaceous additives for sulfur cathode development, an in-house synthesized graphene-based porous carbon (ResFArGO), and a mixture of commercially available conductive carbons (CAs), as a facile and scalable strategy for the development of high-performing LSBs. The additives clearly improve the electrochemical properties of the sulfur electrodes due to an electronic conductivity enhancement, leading to an outstanding C-rate response with a remarkable capacity of 2 mA h cm^{-2} at 1C and superb capacities of 4.3, 4.0, and 3.6 mA h cm^{-2} at C/10 for $ResFArGO_{10}$, $ResFArGO_5$, and CAs, respectively. Moreover, in the case of ResFArGO, the presence of oxygen functional groups enables the development of compact high sulfur loading cathodes (>4 mg_S cm^{-2}) with a great ability to trap the soluble lithium polysulfides. Notably, the scalability of our system was further demonstrated by the assembly of prototype pouch cells delivering excellent capacities of 90 mA h ($ResFArGO_{10}$ cell) and 70 mA h ($ResFArGO_5$ and CAs cell) at C/10.

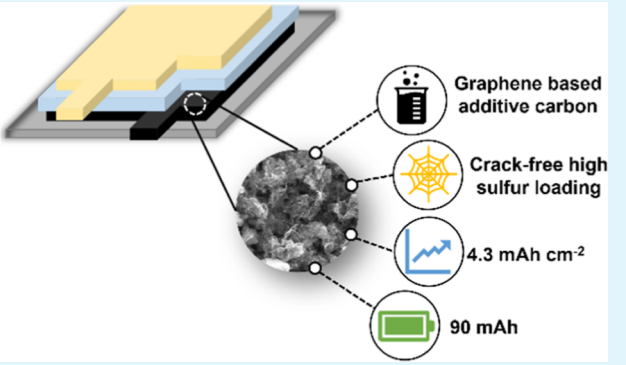

KEYWORDS: *energy storage, lithium−sulfur battery, graphene-based cathodes, high energy density, pouch cell*

1. INTRODUCTION

The development of renewable energy sources and electrification of transport vehicles are considered indispensable strategies nowadays, not only to combat climate change and reduce pollution but also to tackle the current energy crisis due to geopolitical situations. In this scenario, although lithium-ion batteries have dominated the energy storage market since their breakthrough in the 1990s by Sony Company,[1,2] this technology is reaching its theoretical limits. In order to meet the high energy density requirements for electric vehicles with a long driving range and/or cheaper grid/utility energy storage applications,[3] alternative battery technologies have been extensively explored. Among them, lithium−sulfur batteries (LSBs) have attracted the attention of both academia and industry mainly due to the properties of sulfur, such as its abundance (immense stockpiles already exist as a by-product of fossil fuel refining), low-cost, environmental friendliness, high theoretical specific capacity (1675 mA h g^{-1}), and high theoretical energy density (2500 W h kg^{-1}).[4,5] These properties make LSBs potential candidates for lightweight applications, *e.g.*, high-altitude pseudo-satellites or unmanned aircrafts.[6,7] Moreover, as a result of the current uncertain geopolitical situation, the availability and price of essential materials currently used in high energy density batteries (like Ni or Co) are a clear threat to the long-term viability of battery production. Therefore, sulfur is envisioned as a promising alternative solution for the cathode material of future batteries.

However, to become a reality, this technology still needs to overcome several challenges associated with the intricate Li−S chemistry on both metallic lithium anode and sulfur cathode.[7] On the anode side, the most common issues are related to the lithium dendrite/mossy growth that can lead to cell short-

Received: January 20, 2023
Accepted: February 28, 2023
Published: March 16, 2023

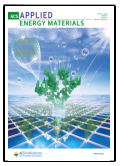

circuiting resulting in safety concerns.[8,9] On the cathode side, several challenges are arising: (i) the insulating nature of both sulfur (S_8, $\approx 10^{-30}$ S m^{-1}) and its final discharge products (*e.g.*, Li_2S with $\approx 10^{-14}$ S m^{-1}); (ii) the large volume expansion from pristine S_8 to Li_2S (≈80%), which can compromise the structural integrity of the cathode; (iii) the high solubility of long-chain lithium polysulfides (LiPS corresponding to Li_2S_n, where $4 \leq n \leq 8$) intermediates and their diffusion through the electrolyte from the cathode to anode inducing the so-called "shuttle effect", resulting in the capacity fading and cell degradation due to the loss of active materials and possible poisoning of the lithium anode.[10,11]

With the aim of tackling these challenges, several strategies including innovative anode architectures and protection techniques,[12−14] functionalized separators,[15−18] liquid electrolyte design,[19−22] the use of all-solid-state polymer electrolytes,[23−26] or novel cathode materials[26−31] have been recently explored. Among them, the sulfur cathode design has been under high scrutiny as it could solve many of the above-mentioned issues. LSB cathodes usually comprise sulfur as the active material, a polymeric binder that agglutinates all the electrode components and ensures their adhesion to the aluminum current collector, and a conductive carbon to allow electron transport through the surface of the insulating sulfur and initiate the redox reactions. Furthermore, the carbonaceous source is not only limited to the role of electronic conductor but can also help to host large amounts of sulfur, buffer the volume changes of sulfur, and act as a polysulfide anchor to reduce its diffusion in the media due to its porous properties. These properties make carbonaceous materials extremely relevant to circumvent the drawbacks derived from the Li−S technology.

Porous carbons with a high specific surface area are the most popular choice for LSBs.[32] Among them, Ketjenblack EC-600JD (KJ600) has been widely used as a carbonaceous compound for Li−S cathode preparation.[33] However, its moderate electronic conductivity and unsuitable porous structure for LiPS retention have pushed researchers to explore novel porous carbon nanostructures with tailored properties.[34] Nevertheless, most of the advanced cathodes involve complex synthetic approaches or sophisticated compounds which would increase the cost of the electrodes.[35−37] In addition, despite the remarkable efficiency provided by these novel materials, it is worth noticing that they may not be scalable for industrial applications, keeping the gap between lab-scale cells and prototyping cells unclosed.[38] Therefore, a facile, scalable, and cheap strategy to improve the electrochemical performance of positive electrodes for LSBs could be the combination of the low-cost KJ600 with some other functional carbonaceous additives. In this regard, our team recently developed a graphene-based activated carbon which was used as the main carbon in the Li−S cathode, allowing the processing of high sulfur loading cathodes with high capacity and high energy density even at the pouch level.[39] Despite the outstanding electrochemical performance, the high production cost is still one of their main limitations. However, its use as an additive in small amounts could effectively reduce the cost of electrode production and make it profitable for LSB manufacturing.

Herein, in this work, we investigate the effect of the incorporation of two different carbonaceous cathode additives in order to obtain high energy density and low-cost LSBs. In the first case, a mixture of commercial additives (CA) containing carbon black (C-65), graphene nanoplatelets (GNP), and multi-walled carbon nanotubes (MWCNTs) is employed. In the second case, an in-house graphene-based activated carbon (ResFArGO) using two different percentages is evaluated as an additive. The electrochemical behavior of these two additive-based cathode formulations is assessed by their C-rate response and long-cycling test under realistic conditions. Finally, the scalability of the strategy is further demonstrated through the assembly of three high-performing 20 cm^2 prototype cells with an active material loading of 4 mg_S cm^{-2}.

2. EXPERIMENTAL SECTION

2.1. Materials. For the preparation of ResFArGO, the same synthesis route detailed in our previous work[29] was followed. Briefly, resorcinol (99 wt %, Sigma-Aldrich) was first dissolved in water and ethanol, and subsequently, commercial graphene oxide (4 mg mL^{-1}, Graphenea) was added under vigorous stirring until complete homogenization. Then, formaldehyde (37 wt %, Sigma-Aldrich) and phosphoric acid were added, and the suspension was swiftly moved to closed recipients into an oven at 85 °C for 70 h to achieve the hydrothermal condensation. After heating the obtained resins at 800 °C in a tubular oven for 1 h under Ar atmosphere, the ResFArGO carbon was obtained. Finally, the carbon was chemically activated, washed, and dried to obtain the final textural properties.

2.2. Electrode Preparation. The sulfur-positive electrodes were prepared according to the following formulation: 64 wt % of sulfur (≥99.0% Sigma-Aldrich), 26 wt % of carbon materials, and 10 wt % of binder based on 5 wt % sodium carboxymethyl cellulose (Sigma-Aldrich)/5 wt % styrene butadiene rubber (Jingrui). In the case of the slurry containing ResFArGO, the 26 wt % of carbon was divided into 16 wt % Ketjenblack EC-600JD (KJ600) and 10 wt % ResFArGO called $ResFArGO_{10}$ or 21 wt % KJ600 and 5 wt % ResFArGO called $ResFArGO_5$ depending on the cathode formulation. On the other hand, the carbon mix in the case of the CA cathode consisted of 16 wt % KJ600, 5 wt % C-65 conductive carbon, 2.5 wt % of MWCNT, and 2.5 wt % of GNP. In all cases, sulfur/carbon composites were prepared *via* the melt diffusion process of 12 h at 155 °C under argon atmosphere. The main difference is that while in the case of the ResFArGO, this process was performed over the carbon mixture, in the case of the cathode with CAs, the melt diffusion was only done with KJ600, and the carbon additives were subsequently added. For the positive electrode preparation, the procedure detailed in our previous work was followed.[39]

Two positive electrodes with different sulfur loadings were prepared depending on their final application: medium mass loading electrodes (~3 mg_S cm^{-2}) used for the C-rate test and high mass loading electrodes (~4 mg_S cm^{-2}) used for the long-cycling test. Electrodes of different sizes were used depending on the battery cell used for the testing: 13 mm in diameter for coin cell and 37.5 × 54 mm electrodes for pouch cell assembly.

2.3. Carbon Characterization. To assess the textural properties of the carbon mixtures, nitrogen adsorption/desorption isotherms at −196 °C were registered with an ASAP2460 instrument from Micromeritics. The specific surface area (S_{BET}) was determined according to the Brunauer−Emmett−Teller equation in the relative pressure range between 0.05 and 0.25, and the pore size distribution (PSD) was obtained using the 2D-NLDFT model and the SAIEUS software. Morphological characterization was performed on a Thermo Fisher Quanta 200 FEG high-resolution scanning electron microscope. The SEM was coupled with an energy dispersive X-ray spectrophotometer from EDAX (Apollo 10) which enables us to solve a wide variety of elemental composition analyses. X-ray photoelectron spectroscopy (XPS) using a Phoibos 150 XPS spectrometer and a non-monochromatic Mg Kα source ($h\nu$ = 1253.6 eV) was performed, aiming to analyze the existing functional groups of the analyzed carbonaceous materials. The spectra were calibrated by assigning graphitic carbon (reference peak) at a binding energy of 285 eV. In

https://doi.org/10.1021/acsaem.3c00177
ACS Appl. Energy Mater. 2023, 6, 3579−3589

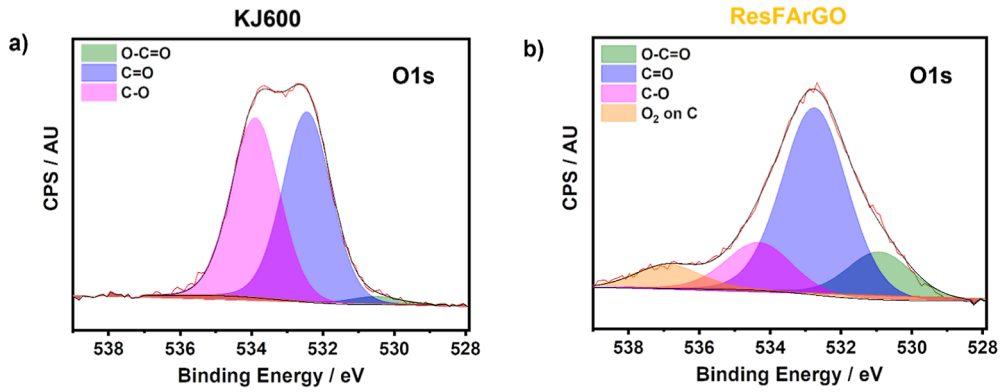

Figure 1. O 1s regions corresponding to XPS spectra of (a) KJ600 and (b) ResFArGO carbonaceous materials.

this case, O 1s and C 1s peaks were fitted using Voigt functions (70% Gaussian and 30% Lorentzian) using the CasaXPS software.

For the LiPS adsorption test, Li_2S_6 solution was prepared by mixing stoichiometric amounts of S_8 and Li_2S in 1,2-dimethoxyethane (DME) to obtain a final concentration of 5 mM. Once the solution was achieved, 10 mg of carbon mixtures was added to 2 mL of Li_2S_6 solution. Subsequently, the different solutions were filtered to eliminate the presence of any solid. The measurements of optical adsorption for the different supernatant solutions were performed on a Cary 5000 UV−vis spectrophotometer (Varian).

2.4. Kinetic Study. In order to fully characterize the kinetic properties of the different carbon mixtures, Li_2S nucleation and dissolution tests were done. The Li_2S_8 solution (0.2 mol L^{-1}) was prepared by stoichiometrically mixing S_8 and Li_2S powder in tetraglyme under vigorous stirring for 3 days. KJ600 reference, CAs, and ResFArGO containing sulfur-free free-standing cathodes with different ratios were prepared following the procedure described above, which were employed as working cathodes coupled with the Li^0 as the anode and Celgard 2500 as the separator. To finally assemble the coin cell, 20 μL of the Li_2S_8 solution was dropped into the cathode part as a catholyte, and then, 20 μL of control anolyte without Li_2S_8 was dropped on the anode side. To carry out the nucleation test, the cells were discharged to 2.06 V under a constant current of 0.112 mA to consume most of the high-order polysulfides and were later maintained at 2.05 V until the current was below 10^{-5} A to induce the nucleation and growth of Li_2S. In the case of the dissolution test, the cells were first discharged to 1.7 V employing a constant current of 0.112 mA to produce Li_2S and then potentiostatically charged at 2.4 V until the current was below 10^{-5} A, looking for the dissolution of Li_2S into higher order LiPS. In both tests, based on Faraday's law, the whole displayed current was used to determine the Li_2S nucleation and dissolution process.

2.5. Electrochemical Performance. The coin cells were assembled in an argon-filled glovebox using the above-outlined S@C electrodes, 16 μm Celgard 1208 as the separator, and Li^0 disk (China Energy Lithium, 500 μm) as the anode. For the pouch cell tests, Celgard 2500 and 39 × 55 mm Li^0 anode were used. In both coin and pouch cells, the employed liquid electrolyte was a 0.5 M lithium bis-(trifluoromethanesulfonyl)imide (99.9 wt %, Solvionic) and 0.5 M lithium nitrate ($LiNO_3$ 99.99 wt %, Sigma-Aldrich) solution in DME/1,3 dioxolane (1:1 in vol), keeping an electrolyte-to-sulfur ratio (E/S) of 7 μL mg^{-1}. As mentioned above, 3 mg_S cm^{-2} loading electrodes was used to carry out the C-rate test, being cycled at C/20, C/10, C/5, C/2, 1C, and C/10. In the case of 4 mg_S cm^{-2} electrodes, the cells were cycled under the long-cycling test at C/10 with 2 preconditioning cycles at C/20. All the battery cycling tests were conducted in a Maccor battery tester, using a cut-off voltage range between 2.6 and 1.7 V. Cyclic voltammetry analyses were performed on a BioLogic VMP3 electrochemical potentiostat making use of the three-electrode setup. The Li^0 disk was used as both a counter and a reference electrode.

3. RESULTS AND DISCUSSION

As previously mentioned, this work aims to evaluate the effect of two well-selected carbonaceous cathode additives on the electrochemical performance of LSBs. The first parameter to be studied was the compatibility of the additives with KJ600. Therefore, the characterization of the carbon mixture in the absence of sulfur was carried out by scanning electron microscopy as can be seen in Figure S1. In both cases, a homogeneous distribution of all the components is observed, due to their good compatibility and high affinity. In the case of CAs (Figure S1a), two significant details can be observed in the SEM images. On the one hand, there is good integration of the GNPs within the carbon black, while on the other hand, it is observed how the MWCNTs act as interconnectors, thus generating an electronic pathway between the different particles. In the case of ResFArGO (Figure S1b), SEM images show a uniform flat-shaped structure, well coated by the carbon black particles, which is expected to not only enhance its conductivity but also ensure a smooth lithium-ion diffusion along the surface of the carbonaceous composite.

Moreover, the textural properties of the as-prepared carbon mixtures were studied through an N_2 adsorption/desorption isotherm measured at −196 °C. As displayed in Figure S2, all the carbonaceous samples exhibit a type IV isotherm, according to IUPAC classification,[40] which is ascribed to mesoporous materials. This can be correlated to the mesoporous nature of KJ600 (see Figure S2a). Specific surface areas of 1324, 799, and 1365 m^2 g^{-1} were calculated for KJ600, CA mixture, and ResFArGO mixture, respectively. The decrease in the specific surface area of CAs when compared to the pristine KJ600 is related to the presence of microporous/non-porous materials (GNPs, C-65, and MWCNTs) on its composition. Furthermore, the PSD in Figure S3 shows a heterogenous distribution with pores ranging from 0.6 to 20 nm for all the carbonaceous materials. However, it is worth mentioning that the ResFArGO mixture presents a larger portion of micropores. In addition to the textural characterization, the surface chemistry of the carbon mixture was analyzed by XPS. Figure 1 shows the O 1s spectra of KJ600 and ResFArGO.

The O 1s spectrum of KJ600 shows a bimodal distribution with two peaks centered at 534 and 532 eV, which can be assigned to C−O and C═O groups present on the surface of the main carbon, respectively. On the other hand, the distribution of peaks in the case of ResFArGO is totally different. In this case, an additional peak is observed at 530 eV, in addition to the C═O peak at 532 eV, which is the most

https://doi.org/10.1021/acsaem.3c00177
ACS Appl. Energy Mater. 2023, 6, 3579−3589

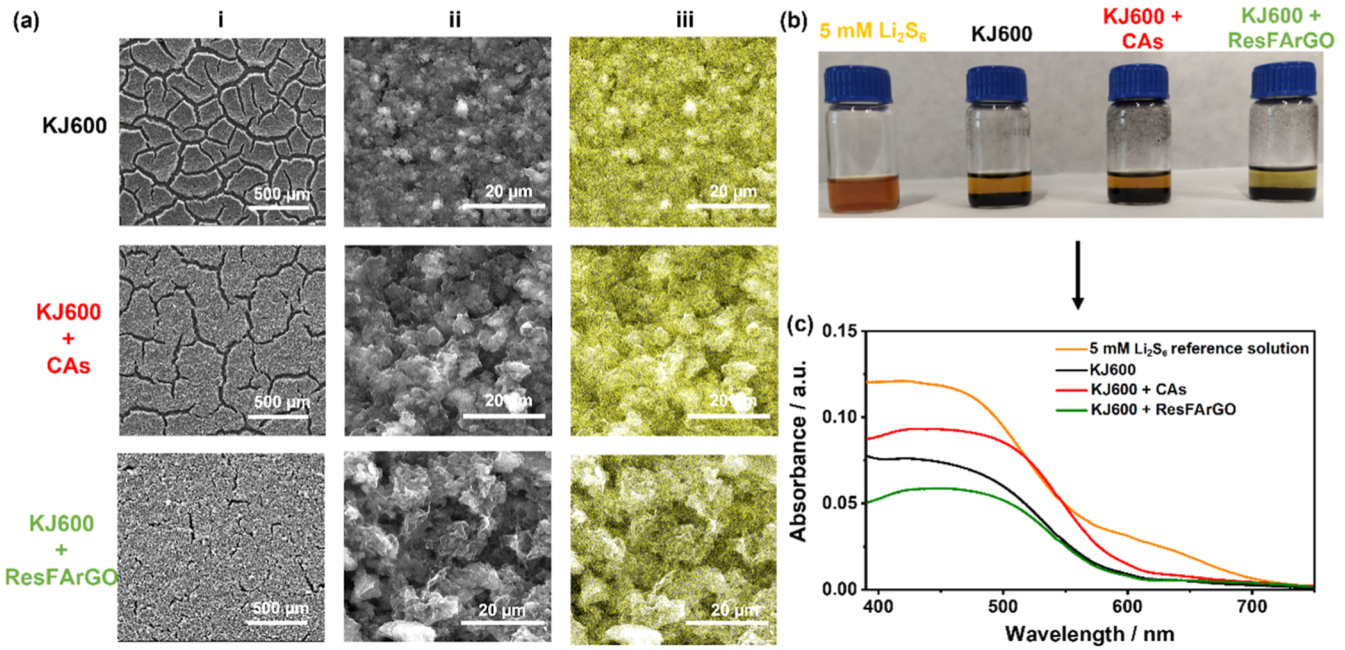

Figure 2. (a) SEM images of the studied high sulfur loading cathode under column (i) low and (ii) high magnifications, and column (iii) EDS sulfur mapping. (b) LiPS adsorption visual test of the analyzed carbon mixtures. (c) UV−vis spectra of the remaining Li_2S_6 solutions after the adsorption test.

predominant peak in this carbon, and the C−O peak centered at 534 eV. This new peak could be assigned to carboxylic acids or esters (O−C═O) present on the carbon surface due to the synthesis process of ResFArGO. As Wasalathilake *et al.*[41] determined through a computational analysis and as has been experimentally confirmed by several studies,[42−50] the remaining surface groups become particularly important since they can play a key role in the development of the cathode owing to its anchoring properties for LiPS and, with that, preventing the subsequently formed LiPS from dissolving in the electrolyte during cycling. The results obtained for the carbon mixtures, shown in Figure S4a,b, follow the same trend as that obtained by the main carbon previously discussed. Furthermore, the oxygen content was also determined from the atomic concentration of the XPS analysis, showing a significant increase in the ResFArGO sample (Figure S4c). The combination of the oxygen content and the type of chemical functional groups present on the surface of ResFArGO could promote a stronger interaction with LiPS in this sample compared to in KJ600.[41−50]

Subsequently, as described in the Experimental Section, composite cathodes were prepared by the sulfur infiltration within the carbon structures by a well-established melt diffusion process at 155 °C for 12 h. Figure 2a presents the SEM images of the three different composite cathodes with 4 mg_S cm^{-2} loading before cycling. Under lower magnification (Figure 2a(i)), large cracks are observed in the surface of the electrode consisting exclusively of KJ600. This phenomenon has been previously reported and analyzed, which is ascribed to the shrinkage during the drying process, due to the large amount of solvent held by the KJ600@S nanocomposite during the electrode slurry preparation.[51] Moreover, the cracking associated with capillary stresses is expected to be more aggressive for aqueous slurries due to the higher surface tension of water.[26] In the case of the CAs electrode, the presence of cracks is greatly reduced, possibly due to the lower amount of KJ600 in the formulation and reduction of the specific surface area after incorporating the conductive additives. It is worth noting that the ResFArGO-containing electrodes shows greater homogeneity, compaction, and adhesion to the current collector despite its high sulfur loading (4 mg cm^{-2}). These outstanding processable features could be ascribed to the amphophilic nature of ResFArGO due to the presence of functional groups on its surface, as previously shown in the XPS data, which improves its dispersion in water, reducing the formation of agglomerates. Images at higher magnification (Figure 2a(ii)) show highly agglomerated particles within the KJ600 reference electrode. On the other hand, in the CAs electrode, some agglomerates can still be observed but are well packed and interconnected between them. Furthermore, MWCNTs can act as electron conductive bridges between the agglomerates, providing the highly pursued electron pathway along the whole electrode. Moreover, in the case of graphene-based activated carbon cathodes, the uniform and 2D flat-shaped structures of ResFArGO are in close contact with KJ600@S agglomerates, providing a high electrical conductivity typically found in graphene-based activated materials. These SEM images confirm the packing properties depending on the selected additives, highlighting the composition containing ResFArGO in which the mechanical properties found for the purely graphene-containing cathodes[39] are also observed when it is combined with KJ600. Finally, as displayed in Figure 2a(iii), energy-dispersive spectrometry (EDS) elemental mapping of S of the all-prepared electrodes reveals the excellent distribution of the active material within the cathode without the presence of any S clusters, confirming the suitability of the selected S infiltration technique.

LiPS dissolution and the consequent corrosion of the lithium anode is one of the major operational challenges faced by LSBs. Generally, the non-polar nature of electrode materials like carbon materials or binders leads to poor interaction with

https://doi.org/10.1021/acsaem.3c00177
ACS Appl. Energy Mater. 2023, 6, 3579−3589

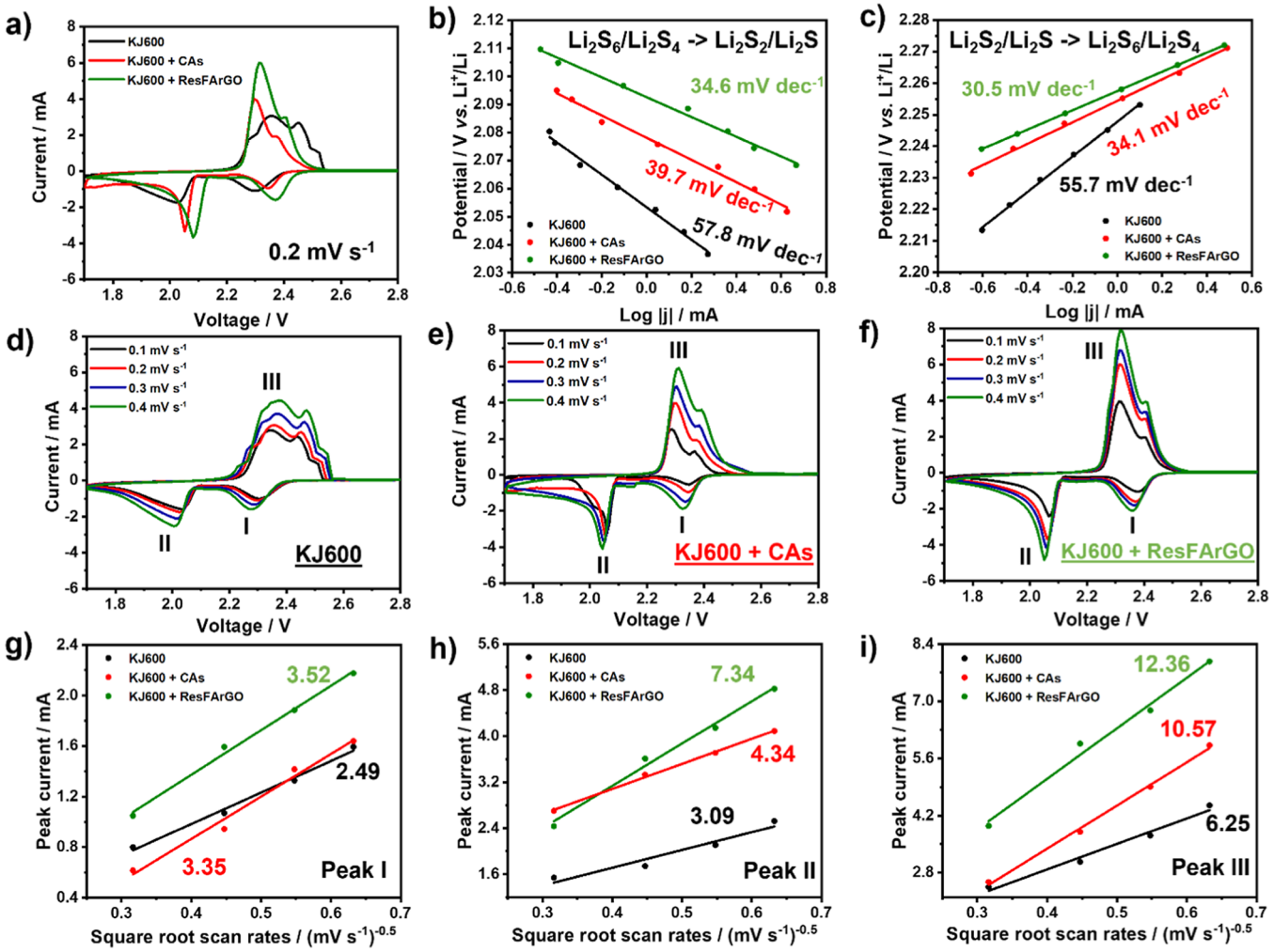

Figure 3. Kinetic study of the KJ600 reference, KJ600 + CAs, and KJ600 + ResFArGO$_{10}$ electrode-based cells: (a) CV in a potential window from 1.7 to 2.8 V at a scan rate of 0.2 mV s^{-1}. (b,c) Tafel plots for the cathodic and anodic conversion reaction, respectively. (d–f) CV curves at different scan rates from 0.1 to 0.4 mV s^{-1}. (g–i) Li$^+$ diffusion behavior analysis.

the polar LiPS, thus failing in their anchoring and compromising the long-term cycling of the battery due to the shuttle effect. In consequence, to analyze the LiPS trapping ability of the all-studied carbon mixtures, a visual test related to the change of the coloration associated with the Li_2S_6 adsorption was performed. In Figure 2b, clear differences in the LiPS trapping ability are observed between each carbon mixture. In the case of the ResFArGO-based mixture, a reduction in the coloration of the solution can be clearly noticed. In the remaining mixtures, although to a less extent, a reduction in the coloration is also detected, indicating that the commercial KJ600 can trap a certain concentration of LiPS. These visual observations were furtherly confirmed by ultraviolet–visual spectroscopy (UV–vis) tests (Figure 2c), in which the same trend is reflected. The expanded UV–vis spectra of all samples are shown in Figure S5.

In order to straighten out the electrocatalytic properties of the studied carbon additives over LSB performance, a wide range of electroanalytical measurements were carried out. First, cyclic voltammetry (CV) profiles of the as-prepared cathodes were performed with a scan rate of 0.2 mV s^{-1} to study the effect of the additives on the redox kinetics. As displayed in Figure 3a, two cathodic peaks can be observed in all cases, the first one around 2.5–2.3 V, which corresponds to the reduction of S_8 to soluble long-chain LiPS (Li_2S_n; where $4 \leq n \leq 8$) and the second one around 2.1–2.0 V ascribed to their successive conversion to insoluble short-chain LiPS (Li_2S_2/Li_2S).[52] Furthermore, in the anodic part, two peaks corresponding to the multistage oxidation from insoluble short-chain LiPS to S_8 with the intermediate formation of the soluble species are also observed.[53] Interestingly, the CV curves show that the addition of either ResFArGO or CAs leads to sharper and higher intensity cathodic peaks, anodic peaks, and reduced polarization (a smaller gap between cathodic and anodic peaks) when compared to the reference KJ600 cathode, which presents broader and lower intensity peaks. These differences in the CV shape can be ascribed to a significant improvement of the kinetics with the presence of the additive. In more detail, the ResFArGO additive cathode presents the sharpest peaks in both cathodic and anodic parts, indicating the fastest reaction kinetics during the redox process compared to the rest of the cathodes. This is in good agreement with the Tafel plots of reduction and oxidation peaks (Figure 3b,c respectively) which were constructed from Figure 3a. The Tafel slopes of both ResFArGO (34.6 and 30.35 mV dec^{-1}) and CA cathodes (39.7 and 34.1 mV dec^{-1}) are considerably lower than the reference cathode (57.8 and 55.7 mV dec^{-1}). These gentle slopes prove the fast Li–S redox

https://doi.org/10.1021/acsaem.3c00177
ACS Appl. Energy Mater. 2023, 6, 3579–3589

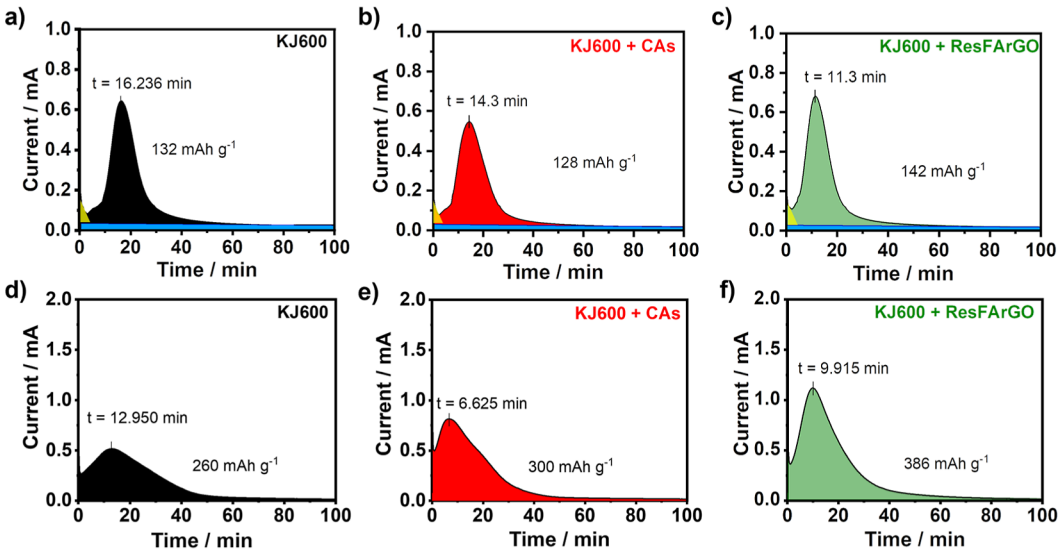

Figure 4. Potentiostatic charge curves of the Li_2S_8 solution to evaluate (a–c) precipitation and (d–f) dissolution kinetics of Li_2S for the three different carbon mixtures.

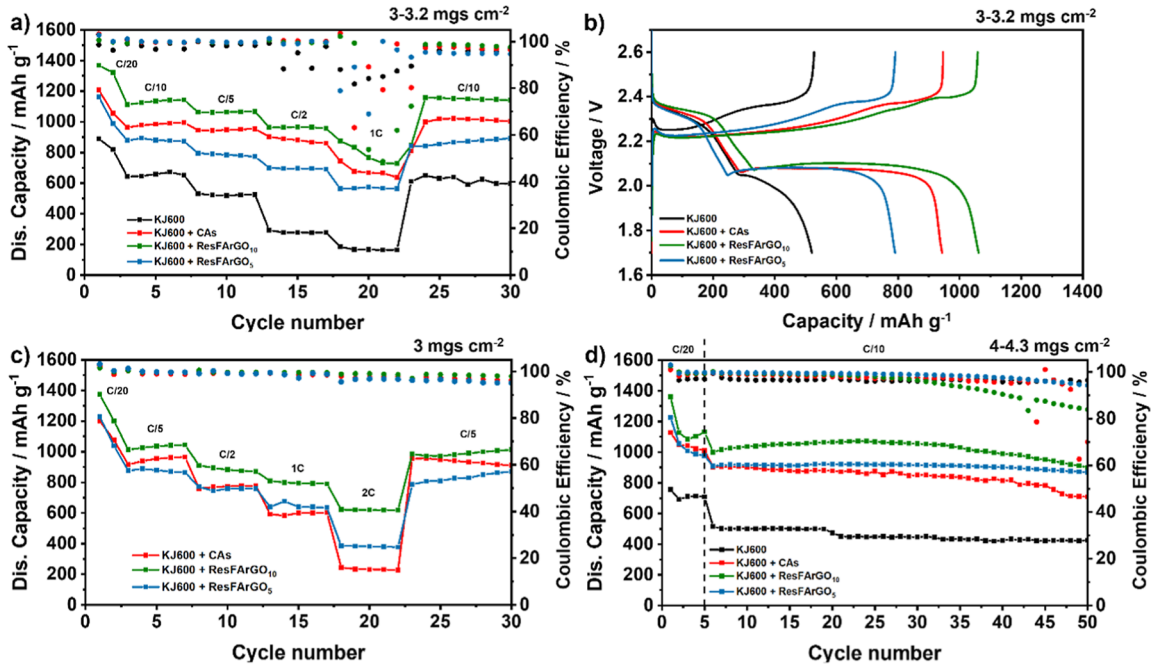

Figure 5. (a) Rate capabilities of Li–S cells using KJ600 as the reference and CAs and ResFArGO additive-based cathode formulations. (b) Galvanostatic discharge/charge profiles of the studied electrodes at C/5. (c) C-rate response of the three systems containing additives using a constant charge rate of C/2. (d) Battery performance of the three studied carbon mixtures and the reference KJ600 in the long cycling test.

reaction, *i.e.*, fast kinetics owing to the enhanced electronic conductive network provided by the additives. Moreover, the superior electrocatalytic properties are also attributed to the improved LiPS anchoring ability provided by the ResFArGO additive. To further analyze the reaction kinetic behavior of the cathodes, CV measurements under different scan rates from 0.1 to 0.4 mV s^{-1} were carried out, as shown in Figure 3d–f. As expected, all intensity values of the anodic and cathodic peaks show a linear correlation with the square root of the scan rate (see Figure 3g–i), and the steepness of the slope illustrates the lithium-ion diffusion coefficient. In each of the analyzed peaks, the additive cathodes present a steeper slope than the reference KJ600 cathode, which corresponds to higher lithium-ion diffusion values, with the ResFArGO additive cathode standing out above all others.

Aiming to complete the work and trying to get a deeper insight into the catalytic activities undergone by the different cathodes, a detailed study on the Li_2S nucleation and dissolution was also performed. Figure 4 presents the kinetic studies of the different cathodes studied through Li_2S nucleation and dissolution tests. Noteworthy, 75% of the theoretical capacity of LSBs arises from the deposition/nucleation processes of the Li_2S from the Li_2S_4 intermediate. Therefore, as shown in Figure 4a–c, potentiostatic nucleation measurements were performed in order to analyze this essential process. The initial monotonically decreasing current is related to the reduction from the remaining higher-order

https://doi.org/10.1021/acsaem.3c00177
ACS Appl. Energy Mater. 2023, 6, 3579–3589

LiPSs to Li_2S_4. The following current peak could be assigned to the nucleation and growth of solid Li_2S.[54,55] In all cases, a sharp and well-defined peak is observed. However, the sample containing ResFArGO exhibits a sharper current peak appearing in a shorter time than the rest of the samples, indicating a faster Li_2S nucleation process. In addition, in Figure 4a−c the integrated area of the current curves, which is related to the nucleation capacity, can also be observed. Notably, the ResFArGO cell delivers a higher Li_2S nucleation capacity of 142 mA h g^{-1} which is higher than the other formulations, displaying a suitable and favored Li_2S deposition and nucleation. These results are in agreement with those shown in Figure 3, which indicate the catalytic effect of carbonaceous composite. Similarly, the potentiostatic charge processes at 2.4 V are shown in Figure 4d−f. It can be noted that the Li_2S-oxidation capacities of additive-based cathodes are much higher than those of the reference and also appear in an early dissolution time, indicating the promoted dissolution of solid Li_2S.[56] In the case of KJ600 + CAs, the Li_2S dissolution peaks appear at shorter times than in the case of ResFArGO; however, for both samples, the onset of dissolution occurs at the same time. The difference in reaching the maximum is more related to the higher dissolution capacity of the cathode with KJ600 + $ResFArGO_{10}$ than the one with KJ600 + CAs (386 *vs* 300 mA h g^{-1}, respectively), which is in line with the observations in Figure 3a. Therefore, in both kinetic studies (see Figures 3 and 4), the cathode containing a mixture of KJ600 and ResFArGO stands out from the rest, exhibiting promoted Li_2S nucleation and dissolution processes.

To further confirm the robustness of additives in the cathodes, Li−S coin cells were assembled with an S loading of around 3 mg_S cm^{-2} and tested at different C-rates (Figures 5a and S6). In addition to the KJ600 reference cathode and taking into account the good properties demonstrated by the ResFArGO carbon composite, it was decided to go further with this additive by reducing its quantity in the cathode formulation. Thus, we fabricated three different cathode formulations containing CAs (KJ600 + CAs), 10 wt % ResFArGO (KJ600 + $ResFArGO_{10}$) and 5 wt % ResFArGO (KJ600 + $ResFArGO_5$). In comparison with the reported works where S loadings are between 1 and 2 mg_S cm^{-2}, this work presents a study with realistic conditions >3 mg_S cm^{-2}. All cathodes containing additives in their formulation deliver higher specific and areal capacities over the entire range of analyzed C-rates compared to reference KJ600 cells (Figure 5a). Furthermore, it is interesting to note the high-capacity retention resulting from the incorporation of the additives when increasing the cycling rate from C/10 to C/2, being 80% in the case of $ResFArGO_{10}$, 79% for $ResFArGO_5$, and 75% for CAs. This improved capacity retention at high rates proves again the fast kinetics of the cathode with the different additives, highlighting the results obtained with ResFArGO for the two different compositions. Strikingly, the cells exhibit outstanding high capacities even at 1C, delivering 800, 680, and 760 mA h g^{-1} for $ResFArGO_{10}$, $ResFArGO_5$, and CAs, respectively. These obtained values represent an areal capacity close to 2 mA h cm^{-2}, 4 times higher than that of the reference cell (Figure S6). Galvanostatic charge/discharge profiles represented in Figure 5b show the two typical discharge plateaus corresponding to the multi-step sulfur reaction mechanism. It can be noted that both additives allow the reduction in the overpotential of the cell compared to the reference KJ600 cathode, with the lowest polarization obtained for $ResFArGO_{10}$ cells (as further seen in Figure S7). This behavior could be ascribed to their LiPS trapping ability and their enhanced catalytic properties, which are in accordance with the results previously reported during the study. However, if the amount of ResFArGO is reduced to 5 wt %, this effect is less significant, surely due to the reduced anchoring ability of the LiPS, which furtherly demonstrates this assumption.

Nevertheless, despite the high capacities obtained at 1C in the cells containing any kind of carbonaceous additive, as shown in Figure 5a, the Coulombic efficiency (CE) is remarkably low at 1C. This is related to the instability issues of the lithium anode side, especially during the charging process, when Li deposition occurs. It is worth mentioning that the current density applied to a 3 mg_S cm^{-2} loading cell at 1C is 5 mA cm^{-2}, which is a challenging harsh cycling condition for the Li metal anode. Li stripping and plating tests confirm that the instability issue is more pronounced with a current density higher than 4 mA cm^{-2} (Figure S8). In order to prove this hypothesis and overcome the stability issues, C-rate cycling tests keeping the charge rate constant at C/2 aiming for a smooth Li deposition were performed for the different cathode formulations, as displayed in Figure 5c. As expected, the stability of the Li−S cell is improved significantly with a high average CE of 99.2% even at a high discharge C-rate of 2 C and delivering remarkable capacities of 620 mA h g^{-1} for $ResFArGO_{10}$, 390 mA h g^{-1} for $FesFArGO_5$, and 230 mA h g^{-1} for CAs. In addition, the improvements in the properties associated with the incorporation of ResFArGO when compared to a reference sample exclusively formed by KJ600 or with CAs, even in such small amounts, is especially evidenced in the high areal capacities.

In an attempt to confirm that the stability issues identified in the C-rate tests at 1C are associated with the anode, a post-mortem study was carried out. The anodes were studied by SEM after charging at 1C and C/2 (Figure 5a,c, respectively). As can be clearly seen in Figure S9, the deposition is more homogeneous and uniformly distributed in the case of the anode after the charge at C/2, without the presence of fibrillar structures.

Therefore, to achieve the highly desired fast charging operation in this system under realistic conditions, future studies will necessarily need to focus on lithium metal anode optimization by either tuning the electrolyte to facilitate a suitable solid−electrolyte interface formation or employing *ex situ* protection strategies.

In order to achieve higher energy density, Li−S cells with 4 mg_S cm^{-2} loading cathodes were prepared and tested at a constant rate of C/10 to study their cycle life (Figures 5d and S10). In line with previous results, the additive-based cathodes show a significant performance improvement in comparison with the reference one. On the one hand, the inclusion of CAs has yielded a high and constant capacity of 850 mA h g^{-1} (around 3.6 mA h cm^{-2}), which almost doubles the reference cell based on KJ600, *i.e.*, 480 mA h g^{-1} (around 1.9 mA h cm^{-2}). This performance improvement can be ascribed to a suitable combination of the one-dimensional structure of MWCNTs and the bi-dimensional structure of the GNPs, which allows the creation of an outstanding electron pathway that promotes redox kinetics. On the other hand, the incorporation of 5 wt % of ResFArGO in the cathode formulation improves the system stability by maintaining the capacity of 840 mA h g^{-1} during cycling. Finally, the increase of the amount of ResFArGO from 5 to 10 wt % in the cathode

https://doi.org/10.1021/acsaem.3c00177
ACS Appl. Energy Mater. 2023, 6, 3579−3589

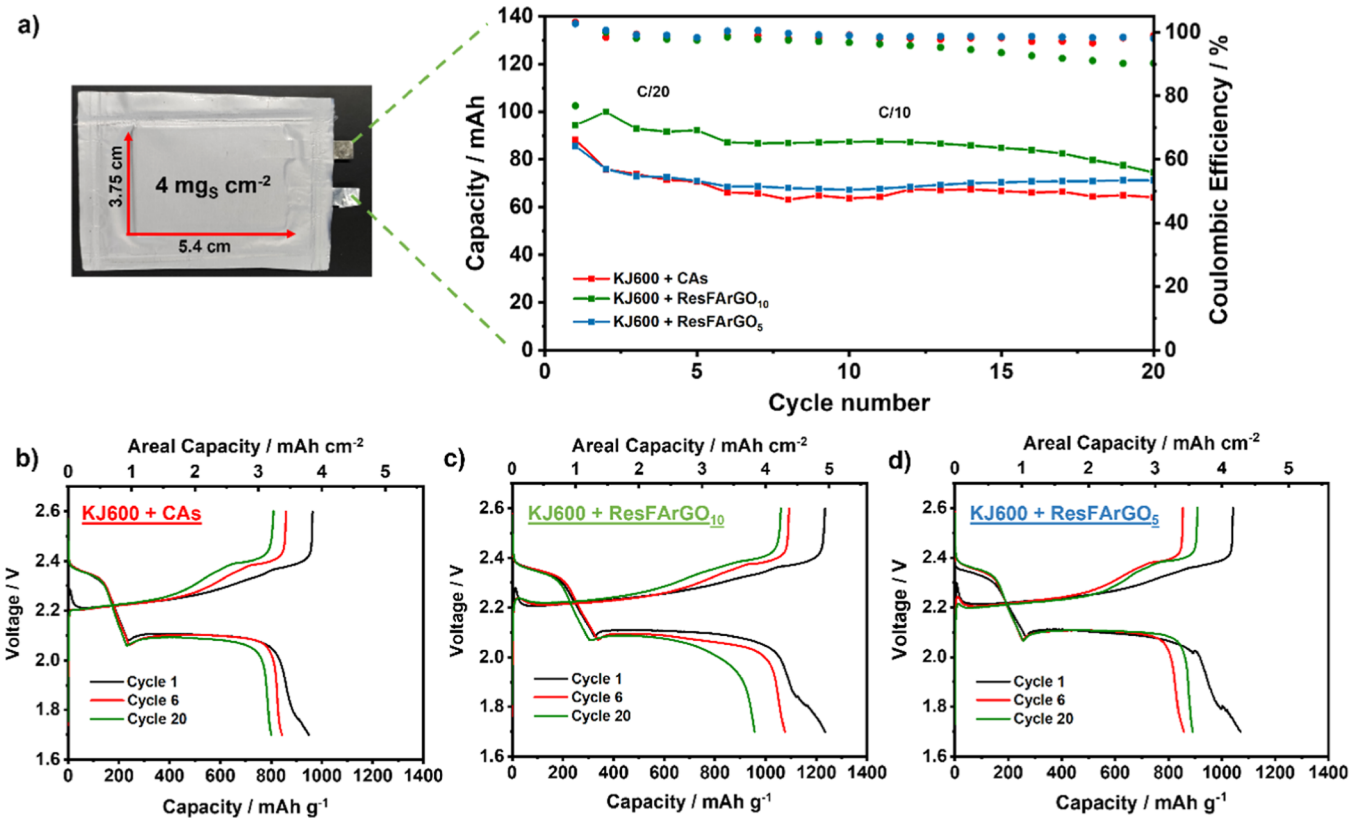

Figure 6. (a) Total capacities of the pouch cells of the three different additive-based cathodes. Discharge/charge profiles of (b) CAs and (c,d) ResFArGO-based pouch cells.

allows for achieving superior S utilization of 1070 mA h g^{-1} (around 4.3 mA h cm^{-2}), thus enabling to reach the areal capacity target set out for Li−S cells to be competitive with traditional Li-ion technologies.[56,57] Likewise, it shows practically stable discharge/charge profiles during the analyzed 50 cycles (Figure S11). Overall, ResFArGO$_{10}$ combines the tailored particle morphology, appropriate textural properties, and surface chemistry that synergistically enhance its LiPS trapping ability and processibility while offering improved electrocatalytic features, with an appropriate cathode formulation which finally benefits the Li−S cell performance. Encouraged by the promising electrochemical performance obtained at the coin cell level associated with the incorporation of these new carbonaceous additives, the evaluation of their performance in a scale-up 20 cm^2 pouch cell was assessed. This step aims at facilitating the direct handover to practical devices and to merge the huge gap between academic research and the industry. As displayed in Figure 6a, it is worth noticing that the obtained performances are quite comparable with the ones obtained in coin cells, with smooth discharge and charge profiles (Figure 6b,c), proving the successful scalability of the system. Furthermore, ResFArGO$_{10}$-based cells stand out again, delivering a remarkably high total capacity of 90 mA h (around, 1100 mA h g^{-1} and 4.4 mA h cm^{-2}) at C/10, while ResFArGO$_5$-based or CAs-based cells reach a similarly notable high capacity of 70 mA h (around, 900 mA h g^{-1} and 3.6 mA h cm^{-2}) at C/10. Although the results are promising in terms of capacity, it should be pointed out that the long-term cyclability at the pouch cell level is far from that required for their deployment in a real application. As has been reported in many of the Li−S pouch cells works,[6,58−60] these cyclability issues are directly related to the lithium anode degradation. On the one hand, the state-of-art liquid electrolyte chosen for battery cycling induces poor long-term lithium anode protection, as $LiNO_3$ is continuously consumed during cycling. On the other hand, it is well known that the lithium anode instability is exacerbated in larger area pouch cells due to the higher total current passing through the electrode, which results in the formation of dead/mossy lithium. Consequently, future works to increase lithium anode stability will be undertaken to guarantee long-term cyclability.

4. CONCLUSIONS

This study showcases and validates the feasibility of the carbonaceous additive incorporation strategy, *i.e.*, CAs and ResFArGO, to a low-cost commercial carbon, such as KJ600, for manufacturing high-performing Li−S cathodes. Consequently, the promising application of these proposed cathodes for LSBs is confirmed by the outstanding electrochemical performances achieved, showing featured reversible capacities of 1070, 880, and 860 mA h g^{-1} for ResFArGO$_{10}$, ResFArGO$_5$, and CAs, respectively, for more than 50 cycles at C/10 with 4 mg$_S$ cm^{-2} mass loading cathodes, and excellent power capability (around, 800 mA h g^{-1} at 1C) in cathodes with a notable S loading of 3 mg cm^{-2}. Finally, due to its promising performance at the lab scale, we demonstrate the scalability and practical applications of these additive-based cathodes by the preparation of a 20 cm^2 pouch cell, which provided in both cases remarkable total capacities of around 90 mA h for ResFArGO$_{10}$ and 70 mA h for ResFArGO$_5$ and CAs, respectively. Both studied additives greatly enhance the S redox kinetics compared to the reference KJ600 as a result, in

https://doi.org/10.1021/acsaem.3c00177
ACS Appl. Energy Mater. 2023, 6, 3579−3589

part, of the improved electronic conductivity and catalysis of the S−S bond cleavage/re-formation. Additionally, the ResFArGO additive is highlighted due to its suitability to trap LiPS ascribed to the functional groups present on its surface together with its ability to develop homogeneous high S loading cathodes even using small amounts of 5 wt %. Finally, taking into account all the results obtained in this work, it could be concluded that the cathode containing a 10 wt % of ResFArGO ($ResFArGO_{10}$) is a promising candidate for the further development of high energy density LSBs. Nevertheless, it has been noted that further work related to the Li anode protection and electrolyte optimization should be done in order to further improve the cycle life of Li−S cells.

■ ASSOCIATED CONTENT

Supporting Information

The Supporting Information is available free of charge at https://pubs.acs.org/doi/10.1021/acsaem.3c00177.

Further details of the carbon characterization, electrochemical characterization of the liquid electrolyte, and full-cell performance of Li−S batteries (PDF)

■ AUTHOR INFORMATION

Corresponding Authors

Alexander Santiago − *Centre for Cooperative Research on Alternative Energies (CIC energiGUNE), Basque Research and Technology Alliance (BRTA), 01510 Vitoria-Gasteiz, Spain;* orcid.org/0000-0003-1267-4224; Email: asantiago@cicenergigune.com

Chunmei Li − *Centre for Cooperative Research on Alternative Energies (CIC energiGUNE), Basque Research and Technology Alliance (BRTA), 01510 Vitoria-Gasteiz, Spain;* orcid.org/0000-0003-4438-0458; Email: cli@cicenergigune.com

Authors

Julen Castillo − *Centre for Cooperative Research on Alternative Energies (CIC energiGUNE), Basque Research and Technology Alliance (BRTA), 01510 Vitoria-Gasteiz, Spain;* Present Address: University of the Basque Country (UPV/EHU), Barrio Sarriena, s/n, 48940 Leioa, Spain; orcid.org/0000-0001-7629-8788

Xabier Judez − *Centre for Cooperative Research on Alternative Energies (CIC energiGUNE), Basque Research and Technology Alliance (BRTA), 01510 Vitoria-Gasteiz, Spain;* orcid.org/0000-0003-2382-2288

Jose Antonio Coca-Clemente − *Centre for Cooperative Research on Alternative Energies (CIC energiGUNE), Basque Research and Technology Alliance (BRTA), 01510 Vitoria-Gasteiz, Spain*

Amaia Saenz de Buruaga − *Centre for Cooperative Research on Alternative Energies (CIC energiGUNE), Basque Research and Technology Alliance (BRTA), 01510 Vitoria-Gasteiz, Spain*

Juan Luis Gómez-Urbano − *Centre for Cooperative Research on Alternative Energies (CIC energiGUNE), Basque Research and Technology Alliance (BRTA), 01510 Vitoria-Gasteiz, Spain;* Present Address: University of the Basque Country (UPV/EHU), Barrio Sarriena, s/n, 48940 Leioa, Spain

Jose Antonio González-Marcos − *Centre for Cooperative Research on Alternative Energies (CIC energiGUNE), Basque Research and Technology Alliance (BRTA), 01510 Vitoria-Gasteiz, Spain;* Present Address: University of the Basque Country (UPV/EHU), Barrio Sarriena, s/n, 48940 Leioa, Spain; orcid.org/0000-0002-5962-7938

Michel Armand − *Centre for Cooperative Research on Alternative Energies (CIC energiGUNE), Basque Research and Technology Alliance (BRTA), 01510 Vitoria-Gasteiz, Spain;* orcid.org/0000-0002-1303-9233

Daniel Carriazo − *Centre for Cooperative Research on Alternative Energies (CIC energiGUNE), Basque Research and Technology Alliance (BRTA), 01510 Vitoria-Gasteiz, Spain;* Present Address: Ikerbasque, Basque Foundation for Science, 48013, Bilbao, Spain.; orcid.org/0000-0002-3591-9792

Complete contact information is available at: https://pubs.acs.org/10.1021/acsaem.3c00177

Author Contributions

A.S., D.C., and C.L. conceived the research, designed the experiments, and supervised the work. J.C., J.L.G.-U., A.S.d.B., J.A.C.-C., and X.J. carried out the experiments and measurements. A.S. and J.C. wrote the initial draft, and all authors contributed to the writing of the final manuscript. The manuscript was written through the contributions of all authors. All authors have given approval for the final version of the manuscript.

Notes

The authors declare no competing financial interest.

■ ACKNOWLEDGMENTS

This work was funded by the European Union's Horizon 2020 research and innovation program Graphene Flagship Core Project 3 (GrapheneCore3) under grant agreement 881603. The project was also supported by Ministerio de Ciencia, Innovación y Universidades (MCIU), Agencia Estatal de Investigación (AEI), and the European Regional Development Fund (ERDF) (RTI2018-098301-B-I00). J.C. is a beneficiary of the Predoctoral Program from the Education Department of the Basque Government. J.L.G.-U. is very thankful to the Spanish Ministry of Universities for the FPU grant (16/03498). Finally, we want to acknowledge GRAPHENEA for supplying the graphene oxide used in this work.

■ REFERENCES

(1) Armand, M.; Tarascon, J.-M. Building Better Batteries. *Nature* **2008**, *451*, 652−657.

(2) Tarascon, J.-M.; Armand, M. Issues and Challenges Facing Rechargeable Lithium Batteries. *Nature* **2001**, *414*, 359−367.

(3) Judez, X.; Eshetu, G. G.; Li, C.; Rodriguez-Martinez, L. M.; Zhang, H.; Armand, M. Opportunities for Rechargeable Solid-State Batteries Based on Li-Intercalation Cathodes. *Joule* **2018**, *2*, 2208−2224.

(4) Zhou, G.; Chen, H.; Cui, Y. Formulating Energy Density for Designing Practical Lithium−Sulfur Batteries. *Nat. Energy* **2022**, *7*, 312−319.

(5) Bruce, P. G.; Freunberger, S. A.; Hardwick, L. J.; Tarascon, J. M. Li-O2 and Li-S Batteries with High Energy Storage. *Nat. Mater.* **2012**, *11*, 19−29.

(6) Dörfler, S.; Althues, H.; Härtel, P.; Abendroth, T.; Schumm, B.; Kaskel, S. Challenges and Key Parameters of Lithium-Sulfur Batteries on Pouch Cell Level. *Joule* **2020**, *4*, 539−554.

(7) Cleaver, T.; Kovacik, P.; Marinescu, M.; Zhang, T.; Offer, G. Perspective—Commercializing Lithium Sulfur Batteries: Are We Doing the Right Research. *J. Electrochem. Soc.* **2018**, *165*, A6029−A6033.

(8) Cheng, X. B.; Zhang, R.; Zhao, C. Z.; Zhang, Q. Toward Safe Lithium Metal Anode in Rechargeable Batteries: A Review. *Chem. Rev.* **2017**, *117*, 10403−10473.
(9) Lin, D.; Liu, Y.; Cui, Y. Reviving the Lithium Metal Anode for High-Energy Batteries. *Nat. Nanotechnol.* **2017**, *12*, 194−206.
(10) Ren, W.; Ma, W.; Zhang, S.; Tang, B. Recent Advances in Shuttle Effect Inhibition for Lithium Sulfur Batteries. *Energy Storage Mater.* **2019**, *23*, 707−732.
(11) Wild, M.; O'Neill, L.; Zhang, T.; Purkayastha, R.; Minton, G.; Marinescu, M.; Offer, G. J. Lithium-Sulfur Batteries, A Mechanistic Review. *Energy Environ. Sci.* **2015**, *8*, 3477−3494.
(12) Liang, X.; Pang, Q.; Kochetkov, I. R.; Sempere, M. S.; Huang, H.; Sun, X.; Nazar, L. F. A Facile Surface Chemistry Route to a Stabilized Lithium Metal Anode. *Nat. Energy* **2017**, *2*, 17119.
(13) Baloch, M.; Shanmukaraj, D.; Bondarchuk, O.; Bekaert, E.; Rojo, T.; Armand, M. Variations on Li3N Protective Coating Using Ex-Situ and in-Situ Techniques for Li° in Sulphur Batteries. *Energy Storage Mater.* **2017**, *9*, 141−149.
(14) Xu, J.; Xu, L.; Zhang, Z.; Sun, B.; Jin, Y.; Jin, Q.; Liu, H.; Wang, G. Heterostructure ZnSe-CoSe2 Embedded with Yolk-Shell Conductive Dodecahedral as Two-in-One Hosts for Cathode and Anode Protection of Lithium−Sulfur Full Batteries. *Energy Storage Mater.* **2022**, *47*, 223−234.
(15) He, J.; Chen, Y.; Manthiram, A. Vertical Co9S8 Hollow Nanowall Arrays Grown on a Celgard Separator as a Multifunctional Polysulfide Barrier for High-Performance Li−S Batteries. *Energy Environ. Sci.* **2018**, *11*, 2560−2568.
(16) Bauer, I.; Thieme, S.; Brückner, J.; Althues, H.; Kaskel, S. Reduced Polysulfide Shuttle in Lithium-Sulfur Batteries Using Nafion-Based Separators. *J. Power Sources* **2014**, *251*, 417−422.
(17) Gao, Z.; Xue, Z.; Miao, Y.; Chen, B.; Xu, J.; Shi, H.; Tang, T.; Zhao, X. TiO2@Porous Carbon Nanotubes Modified Separator as Polysulfide Barrier for Lithium-Sulfur Batteries. *J. Alloys Compd.* **2022**, *906*, 164249.
(18) Wang, X.; Yang, L.; Wang, Y.; Li, Q.; Chen, C.; Zhong, B.; Chen, Y.; Guo, X.; Wu, Z.; Liu, Y.; Liu, Y.; Sun, Y. Novel Functional Separator with Self-Assembled MnO2 Layer via a Simple and Fast Method in Lithium-Sulfur Battery. *J. Colloid Interface Sci.* **2022**, *606*, 666−676.
(19) Nakanishi, A.; Ueno, K.; Watanabe, D.; Ugata, Y.; Matsumae, Y.; Liu, J.; Thomas, M. L.; Dokko, K.; Watanabe, M. Sulfolane-Based Highly Concentrated Electrolytes of Lithium Bis-(Trifluoromethanesulfonyl)Amide: Ionic Transport, Li-Ion Coordination, and Li-S Battery Performance. *J. Phys. Chem. C* **2019**, *123*, 14229−14238.
(20) Weller, C.; Pampel, J.; Dörfler, S.; Althues, H.; Kaskel, S. Polysulfide Shuttle Suppression by Electrolytes with Low-Density for High-Energy Lithium−Sulfur Batteries. *Energy Technol.* **2019**, *7*, 1900625.
(21) Baek, M.; Shin, H.; Char, K.; Choi, J. W. New High Donor Electrolyte for Lithium−Sulfur Batteries. *Adv. Mater.* **2020**, *32*, 2005022.
(22) Liu, J.; Li, S.; Marium, M.; Wang, B.; Ueno, K.; Dokko, K.; Watanabe, M. Towards Practical Cells: Combined Use of Titanium Black as a Cathode Additive and Sparingly Solvating Electrolyte for High-Energy-Density Lithium−Sulfur Batteries. *Sustainable Energy Fuels* **2021**, *5*, 1821−1831.
(23) Garbayo, I.; Santiago, A.; Judez, X.; de Buruaga, A. S.; Castillo, J.; Muñoz-Márquez, M. A. Alumina Nanofilms As Active Barriers for Polysulfides in High-Performance All-Solid-State Lithium-Sulfur Batteries. *ACS Appl. Energy Mater.* **2021**, *4*, 2463−2470.
(24) Li, C.; Zhang, Q.; Sheng, J.; Chen, B.; Gao, R.; Piao, Z.; Zhong, X.; Han, Z.; Zhu, Y.; Wang, J.; Zhou, G.; Cheng, H. M. A Quasi-Intercalation Reaction for Fast Sulfur Redox Kinetics in Solid-State Lithium-Sulfur Batteries. *Energy Environ. Sci.* **2022**, *15*, 4289−4300.
(25) Sheng, J.; Zhang, Q.; Sun, C.; Wang, J.; Zhong, X.; Chen, B.; Li, C.; Gao, R.; Han, Z.; Zhou, G. Crosslinked Nanofiber-Reinforced Solid-State Electrolytes with Polysulfide Fixation Effect Towards High Safety Flexible Lithium−Sulfur Batteries. *Adv. Funct. Mater.* **2022**, *32*, 2203272.
(26) Santiago, A.; Castillo, J.; Garbayo, I.; Saenz de Buruaga, A.; Coca Clemente, J. A.; Qiao, L.; Cid Barreno, R.; Martinez-Ibañez, M.; Armand, M.; Zhang, H.; Li, C. Salt Additives for Improving Cyclability of Polymer-Based All-Solid-State Lithium-Sulfur Batteries. *ACS Appl. Energy Mater.* **2021**, *4*, 4459−4464.
(27) Kensy, C.; Härtel, P.; Maschita, J.; Dörfler, S.; Schumm, B.; Abendroth, T.; Althues, H.; Lotsch, B. v.; Kaskel, S. Scalable Production of Nitrogen-Doped Carbons for Multilayer Lithium-Sulfur Battery Cells. *Carbon* **2020**, *161*, 190−197.
(28) Kensy, C.; Schwotzer, F.; Dörfler, S.; Althues, H.; Kaskel, S. Impact of Carbon Porosity on Sulfur Conversion in Li−S Battery Cathodes in a Sparingly Polysulfide Solvating Electrolyte. *Batteries Supercaps* **2021**, *4*, 823−833.
(29) Han, Z.; Zhao, S.; Xiao, J.; Zhong, X.; Sheng, J.; Lv, W.; Zhang, Q.; Zhou, G.; Cheng, H. M. Engineering D-p Orbital Hybridization in Single-Atom Metal-Embedded Three-Dimensional Electrodes for Li−S Batteries. *Adv. Mater.* **2021**, *33*, 2105947.
(30) Zhang, J.; Zhang, Q.; Qu, X.; Xu, G.; Fan, B.; Yan, Z.; Gui, F.; Yang, L. Hierarchically Pyridinic-Nitrogen Enriched Porous Carbon for Advanced Sodium-Ion and Lithium-Sulfur Batteries: Electrochemical Performance and in Situ Raman Spectroscopy Investigations. *Appl. Surf. Sci.* **2022**, *574*, 151559.
(31) Zhang, X.; Liu, X.; Zhang, W.; Song, Y. Tunable Vacancy Defect Chemistry on Free-Standing Carbon Cathode for Lithium-Sulfur Batteries. *Green Energy Environ.* **2022**, DOI: 10.1016/j.gee.2022.03.006.
(32) Wang, M.; Xia, X.; Zhong, Y.; Wu, J.; Xu, R.; Yao, Z.; Wang, D.; Tang, W.; Wang, X.; Tu, J. Porous Carbon Hosts for Lithium−Sulfur Batteries. *Chem.—Eur. J.* **2019**, *25*, 3710−3725.
(33) Lv, D.; Zheng, J.; Li, Q.; Xie, X.; Ferrara, S.; Nie, Z.; Mehdi, L. B.; Browning, N. D.; Zhang, J. G.; Graff, G. L.; Liu, J.; Xiao, J. High Energy Density Lithium-Sulfur Batteries: Challenges of Thick Sulfur Cathodes. *Adv. Energy Mater.* **2015**, *5*, 1402290.
(34) Kensy, C.; Leistenschneider, D.; Wang, S.; Tanaka, H.; Dörfler, S.; Kaneko, K.; Kaskel, S. The Role of Carbon Electrodes Pore Size Distribution on the Formation of the Cathode−Electrolyte Interphase in Lithium−Sulfur Batteries. *Batteries Supercaps* **2021**, *4*, 612−622.
(35) Liu, H.; Chen, Z.; Man, H.; Yang, S.; Song, Y.; Fang, F.; Che, R.; Sun, D. Template-Guided Synthesis of Porous MoN Microrod as an Effective Sulfur Host for High-Performance Lithium−Sulfur Batteries. *J. Alloys Compd.* **2020**, *842*, 155764.
(36) Strubel, P.; Thieme, S.; Biemelt, T.; Helmer, A.; Oschatz, M.; Brückner, J.; Althues, H.; Kaskel, S. ZnO Hard Templating for Synthesis of Hierarchical Porous Carbons with Tailored Porosity and High Performance in Lithium-Sulfur Battery. *Adv. Funct. Mater.* **2015**, *25*, 287−297.
(37) Wang, B.; Li, T.; Qian, X.; Jin, L.; Yao, S.; Shen, X.; Qin, S. In Situ Growth of Co Nanoparticles in Ketjen Black for Enhanced Electrochemical Performances of Lithium-Sulfur Battery Cathode. *J. Solid State Electrochem.* **2021**, *25*, 1579−1590.
(38) Cleaver, T.; Kovacik, P.; Marinescu, M.; Zhang, T.; Offer, G. Perspective—Commercializing Lithium Sulfur Batteries: Are We Doing the Right Research? *J. Electrochem. Soc.* **2018**, *165*, A6029−A6033.
(39) Jiménez-Martín, G.; Castillo, J.; Judez, X.; Gómez-Urbano, J. L.; Moreno-Fernández, G.; Santiago, A.; Saenz de Buruaga, A.; Garbayo, I.; Coca-Clemente, J. A.; Villaverde, A.; Armand, M.; Li, C.; Carriazo, D. Graphene-based Activated Carbon Composites for High Performance Lithium-Sulfur Batteries. *Batteries Supercaps* **2022**, *5*, No. e202200167.
(40) Thommes, M.; Kaneko, K.; Neimark, A. v.; Olivier, J. P.; Rodriguez-Reinoso, F.; Rouquerol, J.; Sing, K. S. W. Physisorption of Gases, with Special Reference to the Evaluation of Surface Area and Pore Size Distribution (IUPAC Technical Report). *Pure Appl. Chem.* **2015**, *87*, 1051−1069.
(41) Wasalathilake, K. C.; Roknuzzaman, M.; Ostrikov, K.; Ayoko, G. A.; Yan, C. Interaction between Functionalized Graphene and

Sulfur Compounds in a Lithium-Sulfur Battery-a Density Functional Theory Investigation. *RSC Adv.* **2018**, *8*, 2271−2279.
(42) Dhamodharan, D.; Ghoderao, P. P.; Dhinakaran, V.; Mubarak, S.; Divakaran, N.; Byun, H. S. A Review on Graphene Oxide Effect in Energy Storage Devices. *J. Ind. Eng. Chem.* **2022**, *106*, 20−36.
(43) Huang, L.; Zhou, W.; Cheng, S.; Yao, H.; Dong, W.; Li, L.; Ji, X. Preparation of Functional Groups-Rich Graphene Oxide for High-Performance Lithium−Sulfur Batteries. *Mater. Today Sustain.* **2023**, *21*, 100300.
(44) Rong, J.; Ge, M.; Fang, X.; Zhou, C. Solution Ionic Strength Engineering as a Generic Strategy to Coat Graphene Oxide (GO) on Various Functional Particles and Its Application in High-Performance Lithium-Sulfur (Li-S) Batteries. *Nano Lett.* **2014**, *14*, 473−479.
(45) Ji, L.; Rao, M.; Zheng, H.; Zhang, L.; Li, Y.; Duan, W.; Guo, J.; Cairns, E. J.; Zhang, Y. Graphene Oxide as a Sulfur Immobilizer in High Performance Lithium/Sulfur Cells. *J. Am. Chem. Soc.* **2011**, *133*, 18522−18525.
(46) Kim, J. W.; Ocon, J. D.; Kim, H. S.; Lee, J. Improvement of Energy Capacity with Vitamin C Treated Dual-Layered Graphene-Sulfur Cathodes in Lithium-Sulfur Batteries. *ChemSusChem* **2015**, *8*, 2883−2891.
(47) Yu, M.; Ma, J.; Xie, M.; Song, H.; Tian, F.; Xu, S.; Zhou, Y.; Li, B.; Wu, D.; Qiu, H.; Wang, R. Freestanding and Sandwich-Structured Electrode Material with High Areal Mass Loading for Long-Life Lithium−Sulfur Batteries. *Adv. Energy Mater.* **2017**, *7*, 1602347.
(48) Zhang, Y.; Gao, Z.; Song, N.; He, J.; Li, X. Graphene and Its Derivatives in Lithium−Sulfur Batteries. *Mater. Today Energy* **2018**, *9*, 319−335.
(49) Tian, J.; Xing, F.; Gao, Q. Graphene-Based Nanomaterials as the Cathode for Lithium-Sulfur Batteries. *Molecules* **2021**, *26*, 2507.
(50) Zhang, L.; Ji, L.; Glans, P. A.; Zhang, Y.; Zhu, J.; Guo, J. Electronic Structure and Chemical Bonding of a Graphene Oxide-Sulfur Nanocomposite for Use in Superior Performance Lithium-Sulfur Cells. *Phys. Chem. Chem. Phys.* **2012**, *14*, 13670−13675.
(51) Tang, T.; Hou, Y. Chemical Confinement and Utility of Lithium Polysulfides in Lithium Sulfur Batteries. *Small Methods* **2020**, *4*, 1900001.
(52) Du, Z.; Rollag, K. M.; Li, J.; An, S. J.; Wood, M.; Sheng, Y.; Mukherjee, P. P.; Daniel, C.; Wood, D. L. Enabling Aqueous Processing for Crack-Free Thick Electrodes. *J. Power Sources* **2017**, *354*, 200−206.
(53) Zhang, H.; Cui, H.; Li, J.; Liu, Y.; Yang, Y.; Wang, M. Frogspawn Inspired Hollow Fe3C@N-C as an Efficient Sulfur Host for High-Rate Lithium-Sulfur Batteries. *Nanoscale* **2019**, *11*, 21532−21541.
(54) Sun, T.; Zhao, X.; Li, B.; Shu, H.; Luo, L.; Xia, W.; Chen, M.; Zeng, P.; Yang, X.; Gao, P.; Pei, Y.; Wang, X. NiMoO4 Nanosheets Anchored on N-S Doped Carbon Clothes with Hierarchical Structure as a Bidirectional Catalyst toward Accelerating Polysulfides Conversion for Li-S Battery. *Adv. Funct. Mater.* **2021**, *31*, 2101285.
(55) Ye, Z.; Jiang, Y.; Li, L.; Wu, F.; Chen, R. A High-Efficiency CoSe Electrocatalyst with Hierarchical Porous Polyhedron Nano-architecture for Accelerating Polysulfides Conversion in Li−S Batteries. *Adv. Mater.* **2020**, *32*, 2002168.
(56) Yang, Y.; Li, X.; Luo, R.; Zhang, X.; Fu, J.; Zheng, Y.; Huo, K.; Zhou, T. A Topochemically Constructed Flexible Heterogeneous Vanadium-Based Electrocatalyst for Boosted Conversion Kinetics of Polysulfides in Li-S Batteries. *Mater. Chem. Front.* **2021**, *5*, 3830−3840.
(57) Zhao, M.; Li, B. Q.; Peng, H. J.; Yuan, H.; Wei, J. Y.; Huang, J. Q. Lithium−Sulfur Batteries under Lean Electrolyte Conditions: Challenges and Opportunities. *Angew. Chem., Int. Ed.* **2020**, *59*, 12636−12652.
(58) Peng, H. J.; Huang, J. Q.; Cheng, X. B.; Zhang, Q. Review on High-Loading and High-Energy Lithium−Sulfur Batteries. *Adv. Energy Mater.* **2017**, *7*, 1700260.
(59) Zhu, K.; Wang, C.; Chi, Z.; Ke, F.; Yang, Y.; Wang, A.; Wang, W.; Miao, L. How Far Away Are Lithium-Sulfur Batteries From Commercialization? *Front. Energy Res.* **2019**, *7*, 123.
(60) Cheng, X. B.; Yan, C.; Huang, J. Q.; Li, P.; Zhu, L.; Zhao, L.; Zhang, Y.; Zhu, W.; Yang, S. T.; Zhang, Q. The Gap between Long Lifespan Li-S Coin and Pouch Cells: The Importance of Lithium Metal Anode Protection. *Energy Storage Mater.* **2017**, *6*, 18−25.

https://doi.org/10.1021/acsaem.3c00177
ACS Appl. Energy Mater. 2023, 6, 3579−3589